

# Effects of Ru-doping on the magnetism of $\text{Ag}_3\text{LiIr}_2\text{O}_6$ , a candidate Kitaev quantum spin liquid

Sanjay Bachhar,<sup>1,\*</sup> M. Baenitz,<sup>2</sup> John Wilkinson,<sup>3</sup> and A.V. Mahajan<sup>1,†</sup>

<sup>1</sup>*Department of Physics, Indian Institute of Technology Bombay, Powai, Mumbai 400076, India*

<sup>2</sup>*Max Planck Institute for Chemical Physics of Solids, 01187 Dresden, Germany*

<sup>3</sup>*ISIS Pulsed Neutron and Muon Source, STFC Rutherford Appleton Laboratory, Harwell Campus, Didcot, Oxfordshire OX110QX, UK*

(Dated: 2025/03/10)

We report our investigations on  $\text{Ag}_3\text{LiIr}_{1.4}\text{Ru}_{0.6}\text{O}_6$  which results from the Ru substitution in the Kitaev quantum spin liquid candidate  $\text{Ag}_3\text{LiIr}_2\text{O}_6$ . It crystallizes in the monoclinic  $C2/m$  space group like its parent compound,  $\text{Ag}_3\text{LiIr}_2\text{O}_6$ . Our susceptibility measurements reveal an effective moment  $\mu_{\text{eff}} = 2.6 \mu_B$  which is higher than moments of the parent compound and less than that of the Ru-analog ( $\text{Ag}_3\text{LiRu}_2\text{O}_6$ ) suggesting the presence of magnetic  $\text{Ir}^{4+}$  ( $J_{\text{eff}} = 1/2$ ) and  $\text{Ru}^{4+}$  ( $S = 1$ ). Bulk magnetic susceptibility suggests long-range order (LRO) at  $T \sim 20$  K whereas no clear signature is present in the heat capacity. Likewise, there is a loss of the  ${}^7\text{Li}$  NMR spectral intensity around  $T \sim 20$  K as expected at the onset of LRO but a complete wipe out is not seen in contrast to the result in  $\text{Ag}_3\text{LiIr}_2\text{O}_6$ . There is as well a  $T \sim 20$  K anomaly in the  ${}^7\text{Li}$  NMR relaxation rate  $1/T_1$  and also a fall in the  ${}^7\text{Li}$  NMR shift  $K$  with decreasing temperature. These results suggest LRO at  $T \sim 20$  K in  $\text{Ag}_3\text{LiIr}_{1.4}\text{Ru}_{0.6}\text{O}_6$ . However, at low- $T$  below 10 K, we observe a power law variation in magnetic heat capacity  $C_m$  and spin lattice relaxation rate  $1/T_1$ , temperature-independent  ${}^7\text{K}$  and no further loss of the  ${}^7\text{Li}$  NMR spectral intensity. These results might suggest the persistence or stabilisation of a quantum spin liquid-like phase perhaps from a fraction of the sample in  $\text{Ag}_3\text{LiIr}_{1.4}\text{Ru}_{0.6}\text{O}_6$  below 10 K. Our muon spin relaxation  $\mu\text{SR}$  measurements suggest ordering around 20 K consistent with our other probes. It appears that the main effect of Ru-substitution is to shift the LRO to a higher temperature in comparison with  $\text{Ag}_3\text{LiIr}_2\text{O}_6$  though there are signatures of a novel phase below about 10 K.

## I. INTRODUCTION

Kitaev's groundbreaking theoretical proposal that bond-dependent magnetic interactions can stabilize a unique  $Z_2$ -spin-liquid ground state with Majorana excitations, along with the material-specific insights of Jackeli and Khaliullin [1], has driven significant experimental efforts to realize such systems. Their work emphasized that honeycomb lattice structures composed of  $4d/5d$  transition metal oxides, featuring edge-sharing oxygen octahedra and strong spin-orbit coupling, provide the essential ingredients for realizing the Kitaev model [2]. Several potential candidates with such layered honeycomb structures have been explored, including  $\text{Na}_2\text{IrO}_3$  [3],  $\alpha\text{-Li}_2\text{IrO}_3$  (along with its three-dimensional polymorphs) [4], and  $\alpha\text{-RuCl}_3$  [5]. However, these materials exhibit magnetic ordering [6] due to the influence of Heisenberg and other non-Kitaev interactions, limiting the observation of Kitaev interactions to either higher temperatures or when an external magnetic field is applied. An addition to this family is  $\text{H}_3\text{LiIr}_2\text{O}_6$  [7], which is considered as promising spin-orbit-entangled quantum spin liquid [8]. While  $\text{H}_3\text{LiIr}_2\text{O}_6$  exhibits no magnetic ordering down to 0.05 K, the presence of stacking faults between the honeycomb planes complicates its magnetic behavior. Theoretical calculations indicate that bond-

dependent Kitaev interactions play a crucial role, yet Heisenberg and other non-Kitaev interactions cannot be disregarded. These systems are positioned near a tricritical point between ferromagnetic, zigzag, and incommensurate spiral orders, preventing long-range magnetic order [9]. Additionally, the interlayer  $O-H-O$  geometry and the absence of hydrogen ordering significantly influence their magnetic properties [10]. A related Kitaev candidate compound,  $\text{Ag}_3\text{LiIr}_2\text{O}_6$ , replaces hydrogen with Ag as a spacer atom. While some reports suggest Kitaev spin-liquid behavior [11], others indicate an ordered magnetic state [12, 13]. Recent studies, however, provide evidence of a low-temperature ordered phase with persistent spin dynamics [14]. Magnetic order in  $\text{Ag}_3\text{LiIr}_2\text{O}_6$  has been confirmed through muon spin relaxation ( $\mu\text{SR}$ ) and nuclear magnetic resonance experiments. Furthermore, anomalies in the  ${}^7\text{Li}$  shift and spin-lattice relaxation rate around 50 K suggest the presence of short-range correlations. A detailed  $\mu\text{SR}$  analysis reveals a coexistence of incommensurate Néel and striped magnetic environments within the ordered phase. Interestingly, significant quantum fluctuations persist deep into the ordered state, as indicated by an undiminished dynamical relaxation rate. Beyond the choice of a nonmagnetic spacer atom, modifying the in-plane magnetic ion can also lead to novel magnetic phenomena. One such system is  $\text{Ag}_3\text{LiRu}_2\text{O}_6$ , a  $4d^4$ -based compound. R. Kumar et al. [15] suggested it as an  $S = 1$  system, with  $\mu\text{SR}$  measurements revealing spin freezing below 5 K. However, the magnetism remains at the borderline between static and dynamic

\* sanjayphysics95@gmail.com

† mahajan@phy.iitb.ac.in

even at 20 mK, as shown by longitudinal field  $\mu$ SR experiments. In contrast, H. Takagi et al. [16] propose that  $\text{Ag}_3\text{LiRu}_2\text{O}_6$  is a Mott insulator with a  $J_{\text{eff}} = 0$  spin-orbit-entangled singlet state, based on spectroscopic and magnetic studies combined with quantum chemistry calculations. Beyond full substitution of either the spacer or the in-plane magnetic atom, partial substitution offers another intriguing route to tuning magnetism in honeycomb systems. For example, replacing 30% Ru at the Ir site in  $\alpha\text{-Li}_2\text{IrO}_3$  ( $T_N = 15$  K) leads to a complete suppression of long-range order and an enhancement of Kitaev interactions [17]. So, we prepared  $\text{Ag}_3\text{LiIr}_{1.4}\text{Ru}_{0.6}\text{O}_6$  (will be referred to as ALIRO henceforth) containing 30% Ru (4d atom) and 70% Ir (5d atom) on the vertices of the honeycomb to see if a suppression of the Heisenberg interactions can be achieved as in Ru-substituted  $\alpha\text{-Li}_2\text{IrO}_3$ .

Honeycomb lattices are a fertile playground for exploring Kitaev physics. The inter plane spacing can be tuned by changing the spacer atom (H, Ag, or Cu) which has been explored by us. This impacts the magnetic in-plane interactions. Also, the magnetic atoms in the honeycomb plane can be changed (Ir, Ru or a mixture of the two in our case: current paper) to tailor the magnetism of the system. The phase diagram is rich: ranging from the usual ordered state to the Kitaev Spin Liquid state with dynamic moments. Continuing our investigations in this series of systems, we focus in this paper on ALIRO containing  $\text{Ir}^{4+}$  ( $J_{\text{eff}} = 1/2$ ) and  $\text{Ru}^{4+}$  ( $S = 1$ ) with the purpose of looking for possible Kitaev spin-liquid physics as an effect of Ru-substitution.

The remainder of the paper is organised as follows: we start by giving the details on sample preparation and structural characterization (section II) of  $\text{Ag}_3\text{LiIr}_{1.4}\text{Ru}_{0.6}\text{O}_6$ . Following this, bulk magnetization data are presented (section III). Thereafter,  $^7\text{Li}$  nuclear magnetic resonance (NMR) provides further validation of ordering but with additional quantum spin liquid-like features at low- $T$  in section IV. Heat capacity (section VI) does not show any signature of ordering down to 2 K and follows power-law at low- $T$ . Another local probe  $\mu$ SR (section V) suggests magnetic ordering around 20 K. Finally, a comprehensive discussion and conclusions on ALIRO are presented in the sections VII and VIII, respectively.

## II. SAMPLE PREPARATION AND STRUCTURAL DETAILS

The synthesis of  $\text{Ag}_3\text{LiIr}_{1.4}\text{Ru}_{0.6}\text{O}_6$  involves a two-step process similar to its parent compound  $\text{Ag}_3\text{LiIr}_2\text{O}_6$  [14, 18, 19]. In the first step, we prepared  $\alpha\text{-Li}_2\text{Ir}_{0.7}\text{Ru}_{0.3}\text{O}_3$  using the standard solid-state reaction method [17]. After obtaining phase-pure  $\alpha\text{-Li}_2\text{Ir}_{0.7}\text{Ru}_{0.3}\text{O}_3$ , we mixed it with  $\text{AgNO}_3$  in a 1:3 molar ratio and ground the mixture. Subsequently, we heated the mixture at 270°C for 72 hours. In the final step, we washed the product multiple times with deionized water to remove any excess

silver nitrates and by-product  $\text{LiNO}_3$ . We confirmed the absence of excess  $\text{AgNO}_3$  and by-product  $\text{LiNO}_3$  using a solution of KCl.

To check the phase purity as well as crystal structure, we have measured the powder x-ray diffraction (XRD) of polycrystalline  $\text{Ag}_3\text{LiIr}_{1.4}\text{Ru}_{0.6}\text{O}_6$ . The XRD data were collected at room temperature with  $\text{Cu-K}\alpha$  radiation ( $\lambda = 1.54182$  Å) over the angular range  $10^\circ \leq 2\theta \leq 90^\circ$  with a  $0.013^\circ$  step size. Figure 1 shows the single phase

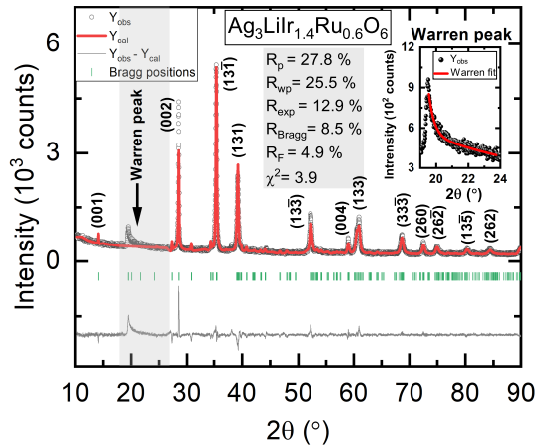


FIG. 1. The single phase Rietveld refinement of XRD pattern (room temperature) of  $\text{Ag}_3\text{LiIr}_{1.4}\text{Ru}_{0.6}\text{O}_6$ . The black open circles are the observed data, the red line is theoretically calculated one, the grey line is the difference between the observed and the calculated data and the green vertical marks are Bragg positions with corresponding Miller indices. Inset shows the Warren peak).

Rietveld refinement of  $\text{Ag}_3\text{LiIr}_{1.4}\text{Ru}_{0.6}\text{O}_6$ . After the refinement, we found that the prepared  $\text{Ag}_3\text{LiIr}_{1.4}\text{Ru}_{0.6}\text{O}_6$  crystallizes in the monoclinic  $C2/m$  space group. There is no sign of unreacted ingredients or impurity phase. From refinement, we obtain the cell parameters of  $\text{Ag}_3\text{LiIr}_{1.4}\text{Ru}_{0.6}\text{O}_6$ ,  $a = 5.26$  Å,  $b = 9.11$  Å,  $c = 6.50$  Å,  $\alpha = \gamma = 90^\circ$ ,  $\beta = 105.9^\circ$ . The goodness of the x-ray refinement is given by the following parameters  $\chi^2 = 3.9$ ,  $R_p = 27.8\%$ ,  $R_{wp} = 25.5\%$ ,  $R_{exp} = 12.9\%$ . Table I summarizes the unit cell parameters and quality factors for the Rietveld refinement of  $\text{Ag}_3\text{LiIr}_{1.4}\text{Ru}_{0.6}\text{O}_6$ . A Warren peak is observed in the range  $19^\circ$  to  $24^\circ$ , shown in inset of Figure 1. Stacking disorder was estimated to be about 7% volume fraction. After excluding the Warren peak, Rietveld refinement is performed with faultless model (stacking faults are ignored) to extract different quality factors, atomic coordinates, site occupancies, and the isotropic Debye-Waller factors ( $B_{\text{iso}} = 8\pi^2 U_{\text{iso}}$ ) of  $\text{Ag}_3\text{LiIr}_{1.4}\text{Ru}_{0.6}\text{O}_6$ , which are tabulated in Table I and Table II, respectively.

As illustrated in Figure 2(a), the crystal structure of ALIRO has a 2D honeycomb network in the  $ab$ -plane, where Ir and Ru atoms occupy the vertices of the honey-

TABLE I. Unit cell parameters and quality factors are reported for the Rietveld refinement of  $\text{Ag}_3\text{LiIr}_{1.4}\text{Ru}_{0.6}\text{O}_6$  at room temperature.

Unit Cell Parameters for space group C2/m		Quality Factors	
a(Å)	5.26(1)		
b(Å)	9.11(6)	$R_{Bragg}$ (%)	8.5
c(Å)	6.50(8)	$R_F$ (%)	4.9
$\alpha = \gamma$ (°)	90	$R_{exp}$ (%)	12.9
$\beta$ (°)	105.9(0)	$R_p$ (%)	27.8
Z	2	$R_{wp}$ (%)	25.5
V (Å <sup>3</sup> )	300.2(6)	$\chi^2$	3.9

TABLE II. Atomic coordinates, Normalized site occupancies, and the isotropic Debye-Waller factors ( $B_{iso} = 8\pi^2 U_{iso}$ ) are reported for the Rietveld refinement of  $\text{Ag}_3\text{LiIr}_{1.4}\text{Ru}_{0.6}\text{O}_6$ .

Atom	Wyckoff position	Site	x	y	z	Norm. Site Occ.	$B_{iso}$ (Å <sup>2</sup> )
Ir(1)	4g	2	0	0.333	0	1.4	0.4
Ru(1)	4g	2	0	0.333	0	0.6	0.4
Li(1)	2a	2/m	0	0	0	1	0.5
O(1)	4i	m	0.417	0	0.22	2	0.5
O(2)	8j	1	0.404	0.322	0.229	4	0.5
Ag(1)	4h	2	0	0.166	1/2	2	0.5
Ag(2)	2d	2/m	1/2	0	1/2	1	0.5

combs and Li is located at the center of the honeycomb. The interlayer spacing between the honeycomb layers is  $c = 6.50$  Å. Figure 2(b) shows the edge shared octahedra where Li and Ir/Ru atoms are situated at the center of the oxygen-octahedral environment. The 3D pi-chart displays the percentage of Ir and Ru. Structural analysis reveals a nearly perfect honeycomb structure with each  $\text{Ir}_{0.7}\text{Ru}_{0.3}$ - $\text{Ir}_{0.7}\text{Ru}_{0.3}$  bond having a length of  $3\text{Å}$  and a bond angle of  $86.9^\circ$  for the  $M - O - M$  ( $M = \text{Ir}_{0.7}\text{Ru}_{0.3}$ ) bond. This is a Kitaev honeycomb geometry, where frustration arises from the bond-dependent interactions. The impact of the presence of  $\text{Ir}^{4+}$  ( $5d^5$ ) and  $\text{Ru}^{4+}$  ( $4d^4$ ) atoms in the honeycomb system on the magnetism is discussed in the following sections.

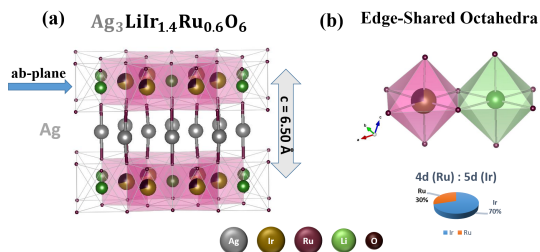


FIG. 2. Crystal structure of  $\text{Ag}_3\text{LiIr}_{1.4}\text{Ru}_{0.6}\text{O}_6$  (a) 3D view of layered material (b) Edge shared octahedra where Li and Ir/Ru sits center of Oxygen-octahedral environment. 3D pi-chart showing the Ir and Ru percentage.

### III. BULK MAGNETIC SUSCEPTIBILITY

The temperature dependence of the susceptibility of ALIRO is displayed in Figure 3 for different zero field cooled (ZFC) and field cooled (FC) modes in various ap-

plied fields. The plot is in a semi-log scale to emphasize the low temperature features. At around 20 K, there is a broad anomaly, possibly due to long range ordering (LRO). We performed Curie-Weiss fitting in the temperature range of 200-400 K to extract Curie constant ( $C = 0.85 \text{ K cm}^3/\text{mol-Ir}_{0.7}\text{Ru}_{0.3}$ ) and a Curie-Weiss temperature ( $\theta_{CW} \sim -165 \text{ K}$ ). The effective magnetic moment of  $\text{Ag}_3\text{LiIr}_{1.4}\text{Ru}_{0.6}\text{O}_6$  is found to be approximately  $2.6 \mu_B$ , which is larger than in  $\text{Ag}_3\text{LiIr}_2\text{O}_6$  ( $\mu_{eff} = 1.76 \mu_B$ ) and smaller than in  $\text{Ag}_3\text{LiRu}_2\text{O}_6$  ( $\mu_{eff} = 2.65 \mu_B$ ), indicating strong antiferromagnetic interaction and magnetic nature of both Ir and Ru. The ZFC-FC bifurcation at various fields suggests frozen magnetism.

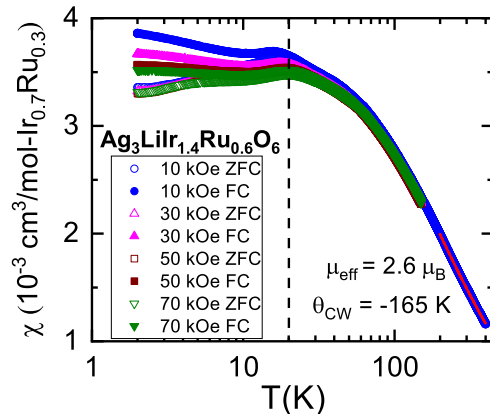


FIG. 3. The temperature dependence of the susceptibility,  $\chi(T) \equiv \frac{M(T)}{H}$  of  $\text{Ag}_3\text{LiIr}_{1.4}\text{Ru}_{0.6}\text{O}_6$  measured in a 10 kOe (blue), 30 kOe (pink), 50 kOe (brown), 70 kOe (green) zero field cooled (ZFC) and field cooled (FC) mode. The open circle symbol represents ZFC data and filled circles are for FC mode data.

### IV. NUCLEAR MAGNETIC RESONANCE

In order to probe the intrinsic magnetic behavior of the correlated  $\text{Ir}^{4+}$ - $\text{Ru}^{4+}$  ions on the honeycomb lattice in  $\text{Ag}_3\text{LiIr}_{1.4}\text{Ru}_{0.6}\text{O}_6$ ,  $^7\text{Li}$  ( $I=3/2$ ,  $\gamma/2\pi = 16.546 \text{ MHz/T}$ ) NMR measurements were carried out.

Figure 4 shows representative NMR spectra at 80 K and 300 K for  $\text{Ag}_3\text{LiIr}_2\text{O}_6$  and  $\text{Ag}_3\text{LiIr}_{1.4}\text{Ru}_{0.6}\text{O}_6$ , respectively. The black solid line at 155.457 MHz is the reference position and used for calculating the fractional shift  $K$ . The increase of the linewidth with decreasing temperature is connected with an increase in the internal field distribution. There is a broadening of the NMR spectra in  $\text{Ag}_3\text{LiIr}_{1.4}\text{Ru}_{0.6}\text{O}_6$  compared to  $\text{Ag}_3\text{LiIr}_2\text{O}_6$ . This indicates that the internal field distribution is larger in  $\text{Ag}_3\text{LiIr}_{1.4}\text{Ru}_{0.6}\text{O}_6$  compared to  $\text{Ag}_3\text{LiIr}_2\text{O}_6$ . These are effects due to Ru-doping at Ir site in the titled honeycomb lattice.

Figure 5 shows the product of the nuclear magnetization  $I$  and temperature  $T$  normalized to the maximum,

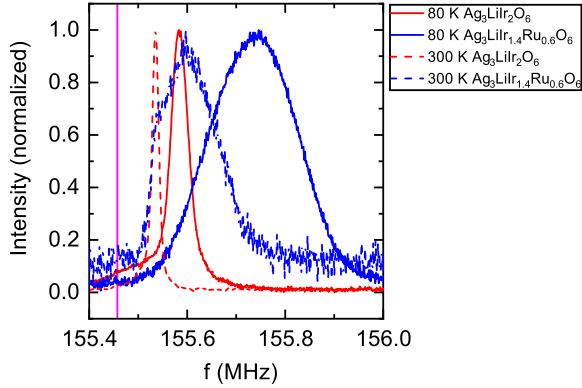


FIG. 4.  ${}^7\text{Li}$  NMR Spectra at 300 K (dot line) and 80 K (solid line) for  $\text{Ag}_3\text{LiIr}_{1.4}\text{Ru}_{0.6}\text{O}_6$  (blue) and  $\text{Ag}_3\text{LiIr}_2\text{O}_6$  (red). The pink line represents reference position at 155.457 MHz.

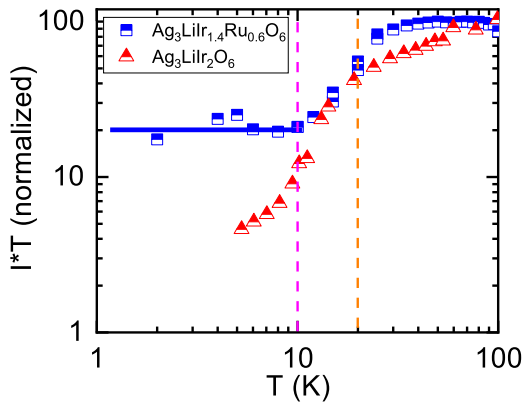


FIG. 5. The product of the nuclear magnetization and temperature normalized to the maximum, as a function of  $T$  for  $\text{Ag}_3\text{LiIr}_{1.4}\text{Ru}_{0.6}\text{O}_6$  (blue square) and  $\text{Ag}_3\text{LiIr}_2\text{O}_6$  (red triangle).

as a function of  $T$  for  $\text{Ag}_3\text{LiIr}_{1.4}\text{Ru}_{0.6}\text{O}_6$  and  $\text{Ag}_3\text{LiIr}_2\text{O}_6$ . We have observed a rapid fall of  $I * T$  at the onset of LRO at  $T \sim 10$  K and also a clear wipe out of the signal in case of  $\text{Ag}_3\text{LiIr}_2\text{O}_6$ . In  $\text{Ag}_3\text{LiIr}_{1.4}\text{Ru}_{0.6}\text{O}_6$ , we observe 80% of  $I * T$  falls in the temperature range 10-30 K and then it remains nearly unchanged below 10 K. The fall in  $I * T$  could be attributed to long range ordering although there is no clear wipe out of signal as observed in  $\text{Ag}_3\text{LiIr}_2\text{O}_6$ . Below 10 K,  $I * T$  remains constant. That could be an indication of the condensation of a new phase (at least from a fraction of the sample) below 10 K.

The NMR resonance shift probes the static intrinsic susceptibility of the system. Figure 6 shows  ${}^7\text{Li}$  NMR shift as a function of temperature in the range 300 K to 2 K for  $\text{Ag}_3\text{LiIr}_{1.4}\text{Ru}_{0.6}\text{O}_6$  which falls in between the two end compounds:  $\text{Ag}_3\text{LiIr}_2\text{O}_6$  and  $\text{Ag}_3\text{LiRu}_2\text{O}_6$ .

The temperature independent behavior of  ${}^7\text{K}$  is one

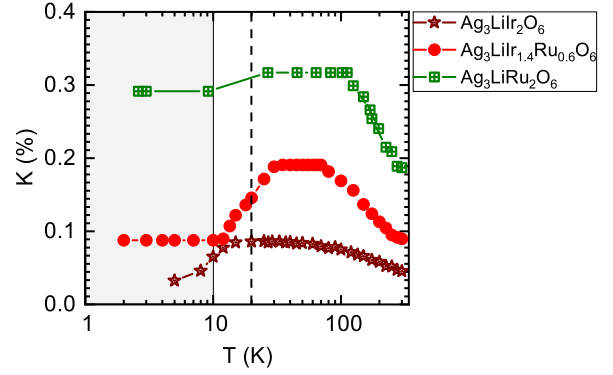


FIG. 6.  ${}^7\text{Li}$  NMR Shift vs.  $T$  for  $\text{Ag}_3\text{LiIr}_{1.4}\text{Ru}_{0.6}\text{O}_6$  (red) in the temperature range 300 K to 2 K. Two end compounds:  $\text{Ag}_3\text{LiIr}_2\text{O}_6$  (brown) and  $\text{Ag}_3\text{LiRu}_2\text{O}_6$  [15] (olive).

of the signatures related to quantum spin liquid-like physics. In  $\text{Ag}_3\text{LiIr}_2\text{O}_6$ ,  ${}^7\text{K}$  falls below 10 K as there was magnetic ordering at  $T \sim 10$  K [14]. In  $\text{Ag}_3\text{LiRu}_2\text{O}_6$ ,  ${}^7\text{K}$  is temperature independent and the system was on the border line of dynamic and static spins as revealed through  $\mu\text{SR}$  studies. In ALIRO,  ${}^7\text{K}$  increases down to 80 K in the paramagnetic region, then a  $T$ -independent region in the temperature range 80-30 K followed by a drop before becoming again  $T$ -independent in the temperature range 10-2 K. The sharp fall around 20 K could be due to LRO. The temperature independent nature of  ${}^7\text{K}$  below 10 K has some signatures of a gapless ground state.

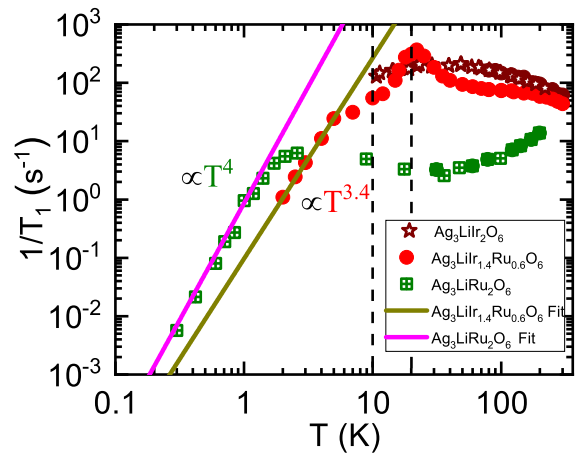


FIG. 7. The Variation of  $1/T_1$  as a function of temperature for  $\text{Ag}_3\text{LiIr}_{1.4}\text{Ru}_{0.6}\text{O}_6$  (red) in the temperature range 300 K to 2 K. Two end compounds:  $\text{Ag}_3\text{LiIr}_2\text{O}_6$  (brown) and  $\text{Ag}_3\text{LiRu}_2\text{O}_6$  [15] (olive).

The spin-lattice relaxation rate,  $(1/T_1)$  measures the  $q$ -averaged imaginary part of susceptibility,  $\chi''(q, \omega_0)/\omega_0$

at a very low-energy  $\omega_0$ , which reflects the density of low-energy spin excitations. We measured  $^7\text{Li}$  spin-lattice relaxation rate ( $1/T_1$ ) for  $\text{Ag}_3\text{LiIr}_{1.4}\text{Ru}_{0.6}\text{O}_6$  by using a saturation recovery method for various temperatures from 300 K to 2 K.

The Figure 7 shows the spin-lattice relaxation rate,  $1/T_1$  as a function of temperature for  $\text{Ag}_3\text{LiIr}_{1.4}\text{Ru}_{0.6}\text{O}_6$  and two end compounds:  $\text{Ag}_3\text{LiIr}_2\text{O}_6$  and  $\text{Ag}_3\text{LiRu}_2\text{O}_6$ . A broad anomaly at  $T \sim 50$  K was observed in  $\text{Ag}_3\text{LiIr}_2\text{O}_6$  indicating of short range ordering followed by a wipe out of the signal below 10 K due to LRO [14]. In  $\text{Ag}_3\text{LiRu}_2\text{O}_6$ , a power-law variation in the spin-lattice relaxation rate indicates gapless excitations. The temperature variation of the spin-lattice relaxation rate,  $1/T_1$  in  $\text{Ag}_3\text{LiIr}_{1.4}\text{Ru}_{0.6}\text{O}_6$  has a broad anomaly at  $T \sim 20$  K followed by a power-law variation at low- $T$ . That indicates long range ordering at  $T \sim 20$  K followed by gapless excitations at low- $T$  through the condensation of a new phase.

## V. MUON SPIN RELAXATION

We have measured zero field (ZF) muon asymmetry in the temperature range 1.5 K to 60 K (Figure 8). We observe a 2/3-loss in the initial asymmetry at the lowest temperature (1.5 K). The high oscillating frequency of muon spins due to static local moments leads to a loss of 2/3- component of initial asymmetry. The fast-falling component could not be capture in the ISIS MUSR instrument which has a pulsed muon source.

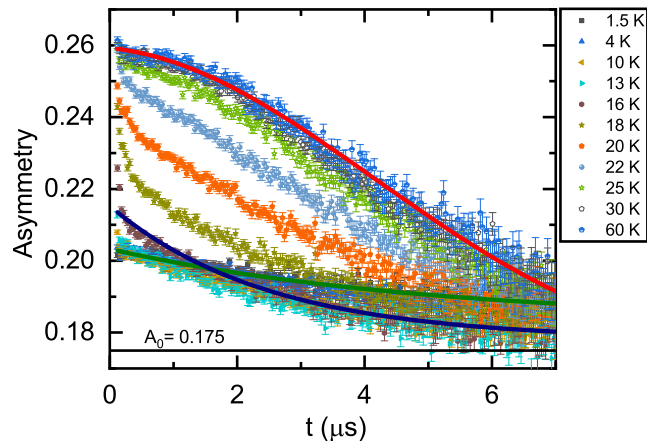


FIG. 8. Variation of the muon asymmetry with time is shown at selected temperatures. Clear 2/3-loss in the initial asymmetry is seen below 18 K indicative of long-range magnetic order. Fits at some representative temperatures are shown as explained in the text.

Remaining 1/3-component of initial asymmetry decays exponentially. Such a loss of initial asymmetry often seen in magnetically ordered system due to large

static spin in ordered state. We find that at temperatures above 20 K, the data are well fit to a product of a static Kubo- Toyabe function with an exponential in addition to a constant background  $A_0$  i.e.,  $A(t) = A_{rel}G_{KT}(\Delta, T)exp(-\lambda t) + A_0$ . Here,  $G_{KT}(\Delta, T)$  is the Kubo-Toyabe function which models the relaxation of muons in a Gaussian distribution of magnetic fields from nuclear moments and  $A_{rel}$  is relaxing asymmetry. From these fits we obtain the field distribution  $\Delta$  to be about 1.8 Oe. This value is typical of nuclear dipolar fields at the muon site, in the present case arising from  $^{107,109}\text{Ag}$ ,  $^6,7\text{Li}$ ,  $^{99,101}\text{Ru}$  and  $^{191,193}\text{Ir}$  nuclei. The exponential term  $exp(-\lambda t)$  arises from the relaxation due to fluctuations of the electronic local moments. Below 20 K, muon asymmetry was well fitted with single exponential in addition to a constant background  $A_0$  i.e.,  $A(t) = A_{rel}exp(-\lambda t) + A_0$ . This relaxation rate  $\lambda(T)$  is small at high temperatures and gradually increases as the local moment fluctuation rate gets smaller (Figure 9). We notice a sharper increase of  $\lambda(T)$  below about 18 K.  $\lambda(T)$  decreases with temperature below 18 K and down to 1.5 K. Below ordering temperature, presence of static spins slow down the muon spin relaxation rate,  $\lambda$ .

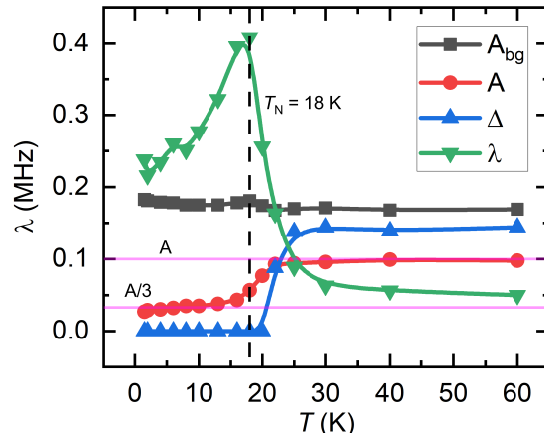


FIG. 9. Variation of the muon relaxation rate,  $\lambda$  as a function of temperature for ALIRO (Green triangle). Static nuclear field distribution,  $\Delta$  is about 1.8 Oe and its variation with  $T$  is shown with blue triangle. Relaxing asymmetry,  $A$  with  $T$  is shown with red circle.  $A$  is constant and no loss down to 25 K. Below 25 K, a fast and a slow component has evolved with lowering temperature. Below 13 K, due to large static field in ordered state, fast component could not observe. The slow component turns out to be 1/3-component of initial asymmetry.  $A_{bg}$  is nearly temperature independent (black square).

## VI. HEAT CAPACITY

To get more information about low energy excitations and ordered phase in ALIRO, we measured the heat ca-

capacity of the sample at constant pressure  $C_p(T)$  at different fields (0-70 kOe) in the temperature range (2-300 K) for 0 kOe and (2-40 K) for other fields. There is no field dependency in heat capacity down to 2 K. Figure 10 shows zero field specific heat,  $C_p(T)$  as a function of temperature for  $\text{Ag}_3\text{LiIr}_{1.4}\text{Ru}_{0.6}\text{O}_6$ ,  $\text{Ag}_3\text{LiIr}_2\text{O}_6$  and non-magnetic analog  $\text{Ag}_3\text{LiSn}_2\text{O}_6$ .

We have created a log-log plot to more clearly show the low-temperature region. In  $\text{Ag}_3\text{LiIr}_2\text{O}_6$ , there was a hint of an ordering peak at  $T \sim 10$  K although the peak is not quite sharp perhaps because of the onset of short range ordering already at  $T \sim 50$  K [14]. There is a clear suppression of the 10 K ordering peak (of  $\text{Ag}_3\text{LiIr}_2\text{O}_6$ ) in  $\text{Ag}_3\text{LiIr}_{1.4}\text{Ru}_{0.6}\text{O}_6$ . In zero-field, the difference between the measured  $C_p$  of the magnetic compound and the  $C_p$  of the non-magnetic analog (that is the lattice contribution) is the magnetic specific heat,  $C_m$  of the compound. The specific heat for  $\text{Ag}_3\text{LiIr}_2\text{O}_6$ ,  $\text{Ag}_3\text{LiIr}_{1.4}\text{Ru}_{0.6}\text{O}_6$  and its non-magnetic analog,  $\text{Ag}_3\text{LiSn}_2\text{O}_6$  match above  $\sim 30$  K. This indicates that the lattice contribution dominates at high temperature. Below 30 K, there are clear differences between  $C_p$  of  $\text{Ag}_3\text{LiIr}_2\text{O}_6$ ,  $\text{Ag}_3\text{LiIr}_{1.4}\text{Ru}_{0.6}\text{O}_6$  and non-magnetic analog,  $\text{Ag}_3\text{LiSn}_2\text{O}_6$ . The calculated  $C_m$  for  $\text{Ag}_3\text{LiIr}_2\text{O}_6$  and  $\text{Ag}_3\text{LiIr}_{1.4}\text{Ru}_{0.6}\text{O}_6$  are plotted in a log-log scale and shown in inset of Figure 10. In the inferred  $C_m$  vs  $T$  of  $\text{Ag}_3\text{LiIr}_2\text{O}_6$ , there is a clear ordering peak around 10 K (more prominent than in the  $C_p$  vs  $T$  plot) and then it follows an exponential decrease. In  $\text{Ag}_3\text{LiIr}_{1.4}\text{Ru}_{0.6}\text{O}_6$ , it is not clear whether the weak anomaly in  $C_m$  vs  $T$  in the range 10-20 K is associated with any frozen magnetism or long range ordering. But, a power law ( $T^2$ ) variation at low- $T$  (below 10 K) in the magnetic heat capacity of  $\text{Ag}_3\text{LiIr}_{1.4}\text{Ru}_{0.6}\text{O}_6$  is observed. This indicates gapless excitations. We speculate that this arises from a new phase which condenses (at least from a fraction of the sample) at low- $T$  [20].

## VII. DISCUSSION

From the extensive range of measurements we have presented, which includes both bulk and local probes, let us now take a look from a broader perspective. We set out with the motivation of suppressing the Heisenberg interaction in  $\text{Ag}_3\text{LiIr}_2\text{O}_6$ , aiming to enhance the anisotropic bond dependent interactions that could promote a Kitaev quantum spin liquid state. Our approach was inspired by previous work on  $\text{Li}_2\text{Ir}_{1-x}\text{Ru}_x\text{O}_3$  [17], where it was demonstrated that substituting 30% Ru in place of Ir could effectively tune the exchange interactions to suppress the ordering. Encouraged by these findings, we pursued the intercalation of  $\text{Li}_2\text{Ir}_{0.7}\text{Ru}_{0.3}\text{O}_3$  with Ag to further explore the effect of structural and electronic modifications on the magnetic properties. Our intercalation experiments were successful, leading to the stabilization of  $\text{Ag}_3\text{LiIr}_{1.4}\text{Ru}_{0.6}\text{O}_6$ . X-ray diffraction and Rietveld refinement suggests that a single phase pure compound has been formed which crystallizes in the C2/m space

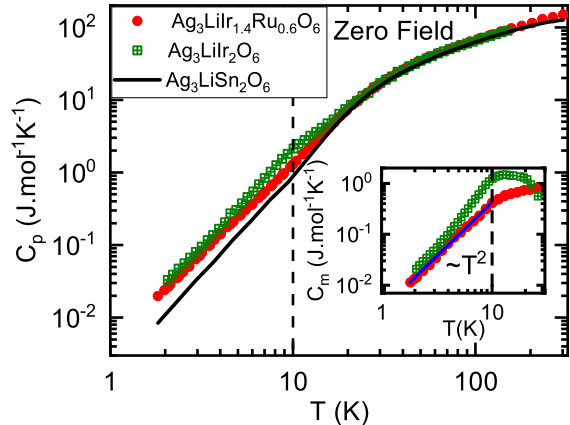


FIG. 10. Specific heat,  $C_p$  as a function of temperature for  $\text{Ag}_3\text{LiIr}_{1.4}\text{Ru}_{0.6}\text{O}_6$  (red circle),  $\text{Ag}_3\text{LiIr}_2\text{O}_6$  (olive square) and non-magnetic analog  $\text{Ag}_3\text{LiSn}_2\text{O}_6$  (black line). (Inset) Magnetic heat capacity comparison between  $\text{Ag}_3\text{LiIr}_{1.4}\text{Ru}_{0.6}\text{O}_6$  (red circle) and  $\text{Ag}_3\text{LiIr}_2\text{O}_6$  (olive square).

group like its parent compound,  $\text{Ag}_3\text{LiIr}_2\text{O}_6$ . The Curie-Weiss temperature was inferred to be  $\sim -165$  K and the effective magnetic moment is found to be approximately  $2.6 \mu_B$ , indicating strong antiferromagnetic interactions and magnetic nature of both Ir and Ru. Presence of magnetic ordering below approximately 20 K in ALIRO was revealed by bulk magnetization, loss in the NMR signal intensity (though not a complete wipe out like in  $\text{Ag}_3\text{LiIr}_2\text{O}_6$ ), anomaly in the  $^7\text{Li}$  spin lattice relaxation rate,  $1/T_1$  and the muon spin relaxation rate,  $\lambda$ . A  $2/3^d$ -loss in the initial zero field muon asymmetry at the lowest temperature (1.5 K), is indicative of a static spin-ordered state. Although ALIRO is magnetically ordered (an **upward** shift in the ordering temperature is an effect of the 30% Ru-substitution at the Ir site in  $\text{Ag}_3\text{LiIr}_2\text{O}_6$ ) like its parent compound,  $\text{Ag}_3\text{LiIr}_2\text{O}_6$  but low- $T$  features are significantly in contrast. Some curious features do show up below 10 K which suggest that a new phase might have been stabilized. In heat capacity, it is not clear whether there is any weak anomaly around 20 K but a  $T^2$  power-law behavior has been observed below 10 K. There is no sign of a complete wipeout of the NMR signal intensity even down to 2 K unlike in  $\text{Ag}_3\text{LiIr}_2\text{O}_6$ . Together with this, a  $T$ -independent NMR shift and a power law variation of  $1/T_1$  are observed below 10 K. These features might suggest condensation of a new spin liquid like phase (at least from a fraction of the sample) at low- $T$ . It is possible that two competitive exchange energies due to the two types of magnetic ions (Ir and Ru) leads to two magnetic phases (long range ordering  $\sim 20$  K and gapless excitations at low- $T$  through condensation of new spin liquid like phase) in different temperature range.

## VIII. CONCLUSIONS

$\text{Ag}_3\text{LiIr}_{1.4}\text{Ru}_{0.6}\text{O}_6$ , a Kitaev honeycomb quantum material containing magnetic  $\text{Ir}^{4+}$  and  $\text{Ru}^{4+}$  shows spin liquid like features at low- $T$  (below 10 K which is below the 20 K ordering temperature) coming from about 20% of non-freezing moments. Muon spin relaxation, nuclear magnetic resonance and magnetization confirms the shift of the ordering temperature to 20 K in  $\text{Ag}_3\text{LiIr}_{1.4}\text{Ru}_{0.6}\text{O}_6$  from 10 K of  $\text{Ag}_3\text{LiIr}_2\text{O}_6$ . Heat capacity,  $^7\text{Li}$ -NMR shift and  $\text{NMR-}1/T_1$  suggests condensation of a spin liquid-like phase at low- $T$  with gapless excitations. Nonetheless, data presented here suggest Ru-substituted  $\text{Ag}_3\text{LiIr}_2\text{O}_6$

to be a strong Kitaev quantum Spin liquid candidate. A single crystal study on this compound could be part of future work.

## IX. ACKNOWLEDGMENT

We thank MOE India, STARS project ID:358 for financial support. We thank Central Facilities at IIT Bombay for support for various measurements. Experiments at the ISIS Neutron and Muon Source were supported by a beam-time allocation RB2220486 from the Science and Technology Facilities Council (<https://doi.org/10.5286/ISIS.E.RB2220486>).

- 
- [1] G. Jackeli and G. Khaliullin, Phys. Rev. Lett. **102**, 017205 (2009), URL <https://link.aps.org/doi/10.1103/PhysRevLett.102.017205>.
- [2] A. Kitaev, pp. 2–111 (2006), ISSN 0003-4916, January Special Issue.
- [3] J. c. v. Chaloupka, G. Jackeli, and G. Khaliullin, Phys. Rev. Lett. **110**, 097204 (2013), URL <https://link.aps.org/doi/10.1103/PhysRevLett.110.097204>.
- [4] S. C. Williams, R. D. Johnson, F. Freund, S. Choi, A. Jesche, I. Kimchi, S. Manni, A. Bombardi, P. Manuel, P. Gegenwart, et al., Phys. Rev. B **93**, 195158 (2016), URL <https://link.aps.org/doi/10.1103/PhysRevB.93.195158>.
- [5] S.-H. Do, S.-Y. Park, J. Yoshitake, J. Nasu, Y. Motome, Y. Kwon, D. T. Adroja, D. J. Voneshen, K. Kim, T.-H. Jang, et al., Nature Physics **13**, 1079 (2017), ISSN 1745-2481, URL <https://doi.org/10.1038/nphys4264>.
- [6] Y. S. Hou, H. J. Xiang, and X. G. Gong, Phys. Rev. B **96**, 054410 (2017), URL <https://link.aps.org/doi/10.1103/PhysRevB.96.054410>.
- [7] S. Bette, T. Takayama, K. Kitagawa, R. Takano, H. Takagi, and R. E. Dinnebier, Dalton Trans. **46**, 15216 (2017), URL <http://dx.doi.org/10.1039/C7DT02978K>.
- [8] K. Kitagawa, T. Takayama, Y. Matsumoto, A. Kato, R. Takano, Y. Kishimoto, S. Bette, R. Dinnebier, G. Jackeli, and H. Takagi, Nature **554**, 341 (2018), ISSN 1476-4687, URL <https://doi.org/10.1038/nature25482>.
- [9] Y. Li, S. M. Winter, and R. Valentí, Phys. Rev. Lett. **121**, 247202 (2018), URL <https://link.aps.org/doi/10.1103/PhysRevLett.121.247202>.
- [10] R. Yadav, R. Ray, M. S. Eldeeb, S. Nishimoto, L. Hozoi, and J. van den Brink, Phys. Rev. Lett. **121**, 197203 (2018), URL <https://link.aps.org/doi/10.1103/PhysRevLett.121.197203>.
- [11] F. Bahrami, W. Lafargue-Dit-Hauret, O. I. Lebedev, R. Movshovich, H.-Y. Yang, D. Broido, X. Rocquefelte, and F. Tafti, Phys. Rev. Lett. **123**, 237203 (2019), URL <https://link.aps.org/doi/10.1103/PhysRevLett.123.237203>.
- [12] F. Bahrami, E. M. Kenney, C. Wang, A. Berlie, O. I. Lebedev, M. J. Graf, and F. Tafti, Phys. Rev. B **103**, 094427 (2021), URL <https://link.aps.org/doi/10.1103/PhysRevB.103.094427>.
- [13] J. Wang, W. Yuan, T. Imai, P. M. Singer, F. Bahrami, and F. Tafti, Phys. Rev. B **103**, 214405 (2021), URL <https://link.aps.org/doi/10.1103/PhysRevB.103.214405>.
- [14] A. Chakraborty, V. Kumar, S. Bachhar, N. Büttgen, K. Yokoyama, P. K. Biswas, V. Siruguri, S. Pujari, I. Dasgupta, and A. V. Mahajan, Phys. Rev. B **104**, 115106 (2021), URL <https://link.aps.org/doi/10.1103/PhysRevB.104.115106>.
- [15] R. Kumar, T. Dey, P. M. Ette, K. Ramesha, A. Chakraborty, I. Dasgupta, J. C. Orain, C. Baines, S. Tóth, A. Shahee, et al., Phys. Rev. B **99**, 054417 (2019), URL <https://link.aps.org/doi/10.1103/PhysRevB.99.054417>.
- [16] T. Takayama, M. Blankenhorn, J. Bertinshaw, D. Haskel, N. A. Bogdanov, K. Kitagawa, A. N. Yaresko, A. Krajewska, S. Bette, G. McNally, et al., Phys. Rev. Res. **4**, 043079 (2022), URL <https://link.aps.org/doi/10.1103/PhysRevResearch.4.043079>.
- [17] H. Lei, W.-G. Yin, Z. Zhong, and H. Hosono, Phys. Rev. B **89**, 020409 (2014), URL <https://link.aps.org/doi/10.1103/PhysRevB.89.020409>.
- [18] S. Bette, T. Takayama, V. Duppel, A. Poulain, H. Takagi, and R. E. Dinnebier, Dalton Trans. **48**, 9250 (2019), URL <http://dx.doi.org/10.1039/C9DT01789E>.
- [19] F. Bahrami, E. M. Kenney, C. Wang, A. Berlie, O. I. Lebedev, M. J. Graf, and F. Tafti, Phys. Rev. B **103**, 094427 (2021), URL <https://link.aps.org/doi/10.1103/PhysRevB.103.094427>.
- [20] P. Khuntia, S. Manni, F. R. Foronda, T. Lancaster, S. J. Blundell, P. Gegenwart, and M. Baenitz, Phys. Rev. B **96**, 094432 (2017), URL <https://link.aps.org/doi/10.1103/PhysRevB.96.094432>.